Rijksuniversiteit Groningen

Bachelor Thesis Astronomy

Galactic paleontology Comparison of the chemical abundances in Halo and Sculptor stars

Jorn Wildering

Supervisor:
Prof. Dr. Eline Tolstoy [a]

July 2, 2021

[a]Kapteyn Astronomical Institute, University of Groningen, The Netherlands

I would like to thank my supervising prof. dr. Eline Tolstoy for her continued support, encouragement, and guidance on this project. I am also very grateful to my friends and family, whom have all helped in uncountable ways.

This work has made use of data from the European Space Agency (ESA) mission *Gaia* (`https://www.cosmos.esa.int/gaia`), processed by the *Gaia* Data Processing and Analysis Consortium (DPAC, `https://www.cosmos.esa.int/web/gaia/dpac/consortium`). Funding for the DPAC has been provided by national institutions, in particular the institutions participating in the *Gaia* Multilateral Agreement.

Abstract

Context. Galactic paleontology studies old, low mass, Metal Poor stars that have lifespans comparable to the age of the universe. The chemical elements in the photospheres of these stars act as records of the chemical processes during the early formation and evolution of galaxies. The Sculptor dSph Galaxy is a very interesting object to study within Galactic paleontology, as it has a population of Metal Poor and Extremely Metal Poor stars, similar to the Galactic Halo, but has markedly lower Carbon abundances than stars in the Galactic Halo. A 2018 paper by Chiti et al. identified a population of Extremely Metal Poor stars, and measured their Carbon over metallicity abundances. Chiti et al. found a Carbon enhanced Extremely Metal Poor fraction of 36%, which they suggest to be comparable to the $\sim$ 42% fraction of Carbon enhanced Extremely Metal Poor stars in the Milky Way Halo. Previous research by Skúladóttir et al. in 2015, had found only a single Carbon enhanced Extremely Metal Poor star. *Aims.* In this paper, we compare the results on Carbon abundances in Sculptor stars of Chiti et al. (2018) with the results from Skúladóttir et al. (2015). We will plot these results in an Aoki diagram to determine the amount of Carbon enhanced Extremely Metal Poor stars in the population of Chiti et al., and compare this to Skúladóttir et al. measurements of Sculptor stars, and Frebel and Norris (2013) measurements on Galactic Halo stars. *Methods.* We perform a sky coordinate match between Chiti et al. (2018) and Hill et al. (2019), and Chiti et al. (2018) and Skúladóttir et al. (2015) to find stars that have been measured in both data sets. We then used these matched stars to compare [C/Fe] and [Fe/H] between Chiti et al. (2018) and Skúladóttir et al. (2015). We calculate luminosities for the population of Chiti et al. and make Aoki diagrams to identify CEMP stars. We also use some additional abundances from Hill et al. (2019) to check the [Ba/Fe] and [Eu/Fe] for some of the matched stars. *Results.* We find 1 CEMP star candidate out of the 100 star population from Chiti et al. (2018). This contradicts their CEMP fraction of 36%. We find increased [C/Fe] values, and lower [Fe/H] values for all matched stars, with exception of stars that previously only had known upper bounds for [C/Fe]. The error margins on [C/Fe] and [Fe/H] are substantial, and require more accurate measurements.

Contents

1 Introduction

When we observe stellar light, the absorption lines in the spectrum can be used to learn about the chemical abundances in the photosphere of the star. The chemical abundances of stellar photospheres can reveal information about the conditions of the interstellar medium out of which the star formed, and the processes that created those elements. We describe those processes with two theories that together explain the creation of all chemical elements. The first is the Big Bang nucleosynthesis, which describes the formation of Hydrogen, Helium, and a small fraction of Lithium. Second; stellar nucleosynthesis, which describes fusion processes in stars and in supernovae, creating all other heavier elements, collectively called "metals" by astronomers. In section 2 we will go over the definition of metals, metallicity and some other vital terms.

As stars have a net effect of producing metals throughout their lifecycle, over time there is an increase in metals in the interstellar medium. We can use this fact to study the early universe, by looking at Metal Poor (MP), or Extremely Metal Poor stars (EMP's). EMP's contain very few metals in their photosphere, which acts as a time capsule by preserving the chemical composition of the interstellar medium out of which the star was formed. This strongly implies that EMP's are significantly older than stars like the sun.

By measuring the chemical abundances of EMP's, we can use the predictive power of stellar nucleosynthesis to place constraints on the conditions of the universe in an earlier time. This makes the study of EMP's very interesting to get a window into the properties and processes of the early universe, such as galaxy formation and evolution (Tolstoy, 2011).

EMP's are notoriously hard to find. Current telescopes can only distinguish very narrow metal lines from individual stars in our Galactic neighborhood. They are most frequently found in the Milky Way Halo, and are generally rare in Dwarf galaxies. Some of the chemical abundances of EMP's in the Milky Way Halo differ from those found in dwarf galaxies.

One notably Metal Poor Dwarf galaxy is the Sculptor Dwarf Spheroidal galaxy (dSph) which has been shown to have a population of Metal Poor stars (Starkenburg et al., 2010; Skúladóttir et al., 2015).

The presence of MP and EMP stars in both the Halo and Sculptor dSph might indicate a common origin. Other chemical trademarks of MP stars, such as relatively high abundances in several of the α elements could also be found in both environments. Alpha elements are chemical elements of even atomic number, e.g. Mg, Si, S, Ca, and Ti made from the nuclei in massive stars. The Carbon abundances do

differ, with high Carbon abundances compared to the Sun being frequent in most MP stars within the Galactic Halo. One group of Carbon rich stars are the so called Carbon-enhanced Metal Poor stars (CEMP's) which are more common in the metal-poor population of the Galactic Halo compared to Sculptor MP stars. Only one star in Sculptor has been confirmed to be a CEMP star by Skúladóttir et al. (2015). This difference in Carbon abundance suggests that a common formation process for the Milky way Halo and Dwarf galaxies is unlikely. Our current understanding of galactic evolution struggles to explain this difference in CEMP fractions of the different stellar regions.

This curious difference between the properties of stars in the Galactic Halo and dwarf galaxy, led to further research on Carbon in Sculptor dSph's stars, and in April 2018 Chiti et al. (2018) published a paper wherein they report a larger population of CEMP stars in Sculptor than previous studies had found. Chiti et al. (2018) measured spectra from a sample of Sculptor stars, selected for EMP stars. They then determined the Carbon abundances. For EMP stars they find a CEMP fraction of 0.36 ± 0.08 Chiti et al. (2018), which they hold in accordance with the ~ 0.42 fraction found for the Milky Way Halo. This fraction of CEMP stars found by Chiti et al. (2018), is also markedly higher than what has been found in other similar investigations. e.g. Kirby et al. (2015) and Skúladóttir et al. (2015).

To investigate this apparent discrepancy between the findings of Chiti et al. and previous research done on Sculptor by Skúladóttir et al. (2015), we compare the results from Chiti et al. (2018), Hill et al. (2019), and Skúladóttir et al. (2015).

From now on we will refer to the data sets of these papers by shorthand notation. We refer to the data set of Chiti et al. (2018) as Chiti, the data set of Hill et al. (2019) as FLAMES (from the FLAMES spectrograph data set with UVES), and the data set from Skúladóttir et al. (2015), as Asa respectively.

We will mainly compare the Carbon abundance, by matching the measured stars in the Chiti paper to earlier measurements. We will also try to match the Chiti stars with additional Marker chemical abundances from FLAMES . In order to put these measurements into context, we will provide a general description of the field of Galactic abundance patterns with a focus on CEMP stars and their function as markers for the conditions of the early evolution of galaxies in section 2. In sections 3 and 4 we will describe the methodology of the matching process and data comparison, and show the results. For section 5 we will discuss the most important points to take away from the results, as well as considerations and shortcomings in the methods. Finally in section 6 we conclude on our findings.

2 Galactic paleontology

2.1 Extremely metal poor stars

Extremely metal poor stars (EMP's) are the living fossils of the stellar kingdom. Galactic paleontology is the field of study that links the properties of EMP stars to earlier stages of galactic evolution. Galactic paleontology can also be called stellar archeology, galactic chemical evolution and near-field cosmology. All use the chemical composition of old stars for clues on early evolutionary processes. To give an indication of how far in the past we can look using old stars, we can estimate stellar lifetimes. Stellar lifetime is proportional to M/L. For stars on the main sequence L is proportional to M^3. So that means stellar lifetime $\tau \approx M^{-2}$.

$$\tau \approx 10^{10}(M_{\odot}/M)^{2.5} yrs \tag{1}$$

τ = stellar lifetime Harwit (1998)

The least massive stars are in the order of a tenth of a solar mass, and thus have lifetimes of about 100 solar lifetimes. Or, using equation 1; $3 * 10^{12}$ years.

This means that low mass stars can have lifetimes comparable, or exceeding the current lifetime of the universe. Photospheres of most low-mass stars are typically very stable chemical environments (McWilliam, 1997), with little to no influx or outflux of external elements, making the photosphere a chemical record of the interstellar cloud out of which the star formed. We can use spectral lines from old stars to gain insight on the chemical environment and processes from the beginning of star formation.

To find old, low-mass, EMP stars we look for stars with weak absorption lines in the IR spectra. The strength of specific absorption lines allows us to determine abundances of chemical elements. In general, the abundance of element A; ϵA is defined as the logarithm of the ratio of that number of atoms of element A; N_A over the number of Hydrogen atoms N_H as shown in equation 2.

$$log_{10}\ \epsilon(A) = log10(N_A/N_H) + 12. \tag{2}$$

It has become standard to express abundances as a ratio relative to solar abundances in the "bracket notation".

$$[A/H] = log10(N_A/N_H)_* - log10(N_A/N_H)_{\odot}, \tag{3}$$

Such that an A abundance of $[A/H] = -3$ corresponds to a 1/1000 the solar abundance.

One particular abundance of note is metallicity. Metallicity is commonly defined to be the abundance of all metals; elements heavier than Helium. In practice, metallicity is typically used to describe the abundance of Iron, and as such is a misnomer. Since we are mainly concerned with finding low metallicity stars, [Fe/H] will be frequently used interchangeably with metallicity. A metallicty of [Fe/H] < -3.0 classifies a star as Extremely Metal Poor (EMP).

By relating the metallicity to the age of the stars we can study the chemical evolution of galaxies throughout different stages of their formation and evolution. Determining an accurate age range for individual stars is complicated. Instead, a general classification system of stellar populations was proposed by Walter Baade in the 1940s that correlates to metallicity and age. In this system, Population Type I stars are young, relatively metal-rich stars, with metallicties comparable to that of the Sun. Population Type II stars are old, Metal-Poor (MP) stars, with metallicities ranging roughly from [Fe/H] = -1.0 to [Fe/H] = -3.0. Although lower metallicities have been found (Starkenburg et al., 2012). The lowest metallicity of Population Type II indicates they formed after only a few stellar generations. Population Type III stars are hypothesized to be first generation stars containing no metals, but are as of yet not demonstrably observed.

By linking metallicity to age, we can study the early universe indirectly by observing properties of MP and EMP stars.

We can use other measurements of those stars to make predictions and constraints on galactic evolution and formation. By measuring proper motions of Population Type II stars, we can learn about the kinematics of the early broader Milky Way. Abundances of chemical elements in turn provide information on the chemical processes of stars in different regions of our galaxy.

One such process is the alpha ladder, or alpha process. The alpha process creates so called alpha elements by alpha particle capture starting from a Carbon seed. It is not to be confused with the triple-alpha process by which Carbon is formed. It occurs in massive stars during the lead-up to a type II supernova. Elements created by this process include O, Ne, Mg, Si, S, Ar, Ca, Ti, and Cr.

Low metallicity stars generally show a relative overabundance of α elements compared to Iron. Stars in the Galactic Halo and dwarf galaxies have comparable abundances in alpha elements.

Carbon abundance measurements for these regions however, differ significantly. This can be seen in the higher fraction of EMP stars within the Galactic halo compared to the Sculptor dwar galaxy that are called to be Carbon-rich Extremely Metal Poor stars, or CEMP stars.

2.2 Carbon enhanced metal poor stars

CEMP stars are Extremely Metal Poor stars that are rich in Carbon. The processes by which these stars attained their Carbon are not yet fully understood. We can look at other chemical abundances in these stars, in order to subdivide CEMP stars by different nucleosynthetic processes. For the purposes of this analysis, we divide CEMP stars into CEMP-s, CEMP-r and CEMP-no stars.

CEMP-s stars are stars enriched by the slow neutron capture process, or s-process. The s-process occurs in asymptotic giant branch (AGB) stars. The excess carbon in CEMP-s stars is thought to originate from an AGB binary companion star (Sharma et al., 2018). Though their Carbon excess can be explained in this way, the chemical composition of these stars does not reflect the ISM out of which the star was formed, and as such, CEMP-s stars do not accurately portray abundance ratios in the ISM of the time they were first formed. A chemical marker that is often used to tell CEMP-s stars apart from other CEMP stars is Barium. EMP-s stars have [Ba/Fe] > 1 and [Ba/Eu] > 0.5.

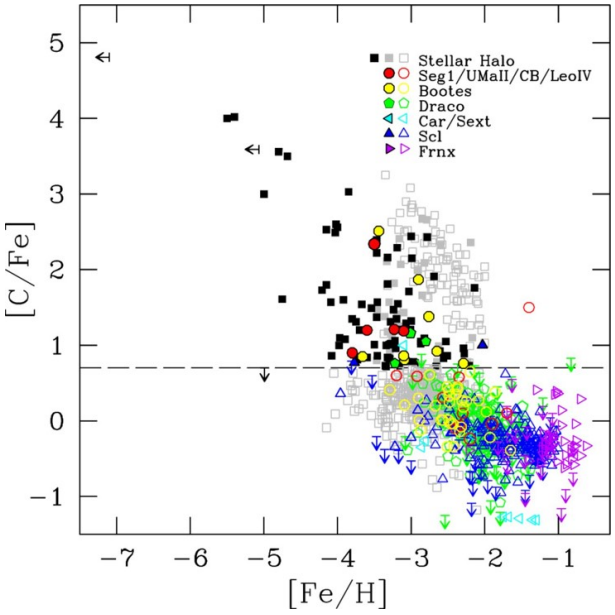

Figure 1: Compilation of stars from Salvadori et al. (2015) with measured [C/Fe] and [Fe/H] in the stellar halo (squares), ultra-faint dwarf galaxies (circles, hexagons, pentagons) and classical dSph galaxies (triangles). [C/Fe] measurements are corrected to account for internal mixing processes (see text). CEMP-no stars are shown as filled symbols, upper limits with arrows. Stars with [C/Fe] > 0.7 and open symbols are CEMP-s/r stars. Filled grey squares are CEMP stars with no available measurements of r- or s-process elements. Colors/symbols identify stars in dwarf galaxies with increasing total luminosity: from red to blue (see labels and text).

CEMP-r stars are stars enriched by the rapid neutron capture process. It is a "rapid" version of the s-process. r-process elements are thought to originate from a combination of separate events. Mainly, in the cores of massive stars undergoing supernovae, and neutron star mergers (Skúladóttir and Salvadori, 2020). CEMP-r stars have [Eu/Fe] $> +1$ and [Ba/Eu] < 0. Europium is almost exclusively formed by the rapid process (Côté et al., 2018).

Finally, there are CEMP-no stars. The "no" in CEMP-no stars refers to no r-process or s-process enhanced elements. We do not currently know the exact cause of their Carbon enhancement. The Carbon abundance in CEMP stars is likely the cause of several nucleosynthetic sources (Lardo et al., 2016). They are possibly formed out of Carbon enhanced gas clouds, enriched by low/no metallicity stars (Sharma et al., 2018). CEMP-no stars are of particular interest when trying to learn about the chemical evolution of different regions in our Galactic neighborhood.

To investigate the CEMP-no fraction in the data set of Chiti et al. (2018), we will use the definition of CEMP stars from Aoki et al. (2007).

1. $[C/Fe] \geq +0.7$ for stars with $\log(L/L\odot) \leq 2.3$
2. $[C/Fe] \geq +3.0 - \log(L/L\odot)$ for stars with $\log(L/L\odot) > 2.3$

In section 4.2 we plot this function in relation to Chiti's data set to find CEMP star candidates. In section 4.3, we show our findings on the [Ba/Fe] and [Eu/Fe] values for some of the stars we were able to match between Chiti et al. (2018) and Hill et al. (2019).

2.3 Measuring Carbon abundance

The process of measuring abundances involves spectroscopic measurements on the strength of different absorption lines. For Carbon specifically, this poses a challenge, as the abundances of Carbon in EMP stars are generally low, and the Carbon spectral lines are weak. There are several methods research groups have used to estimate Carbon abundances in EMP stars, but for the purpose of this paper we will only go over the vary basics in very general terms.

To measure Carbon abundance, researchers measure other molecular spectral lines that can be related to Carbon. Using models of the molecular and chemical interactions in the photospheres of stars, we can predict the ratios of certain molecules. These predictions do require us to make assumptions. An example of the assumptions made to measure the [C/Fe] in Skúladóttir et al. (2015) is given in section 3.2.

3 Methods

3.1 Matching

3.1.1 Matching data sets

In order to investigate the results from Chiti et al. (2018) in more detail, we first need to match spectroscopy observations on Sculptor stars from different research

groups to the Chiti sample. We do this using the sky-coordinates of the sample stars, and will also need those samples to include [Fe/H] and [C/Fe] measurements for our comparisons. It is important to have an accurate matching process, as each research group has their own star naming conventions. By matching the sky-coordinates we can identify which stars have been measured in both samples and compare the results.

We will be using Hill et al. (2019) and Skúladóttir et al. (2015). Jablonka et al. (2015) have determined chemical abundances for a large number of elements, but lack a [C/Fe] measurement. Skúladóttir et al. (2015) does have [C/Fe] estimates, including a measurement on the only known star in Sculptor that falls under the definition of a CEMP-no star; ET0097, before the Chiti et al. (2018) results, which we will use several times as a reference.

FLAMES data (from the FLAMES VLT fibre facility), which contains measurements on Sculptor stars from Frebel et al. (2010), Tafelmeyer sample, Starkenburg sample, Jablonka et al. 2015, and Simon et al. 2015, as well as with Asa data from table 6 in Skúladóttir et al. 2015 paper.

3.1.2 Matching process

We compared the sky coordinates of the stars in the Chiti et al. paper from their table 6, with FLAMES, and Asa.

We used the Topcat (Tool for OPerations on Catalogues And Tables) (Taylor, 2005, 2006) software for a sky coordinate match of the Chiti, FLAMES and Asa data. Before the matching process, right ascension and declination of the different tables were all converted to arcseconds. We sometimes also refer to right ascension and declination by degrees when convenient. With 1 degree = 3600 arcseconds.

The error margins on position are in the order of $\pm$ 1 arcsecond. We chose a matching radius of $\pm$ 2 arcseconds to match Chiti and FLAMES stars. Then, we did the same for Chiti and Asa. For the sky pixel size setting in Topcat, we use a tuning of 20 corresponding to 0.2 arcseconds pixels. Figure 2 shows the skycoordinates plot of a zoomed in field of view of the Sculptor dSph Galaxy containing all the matched stars.

3.1.3 Matching results

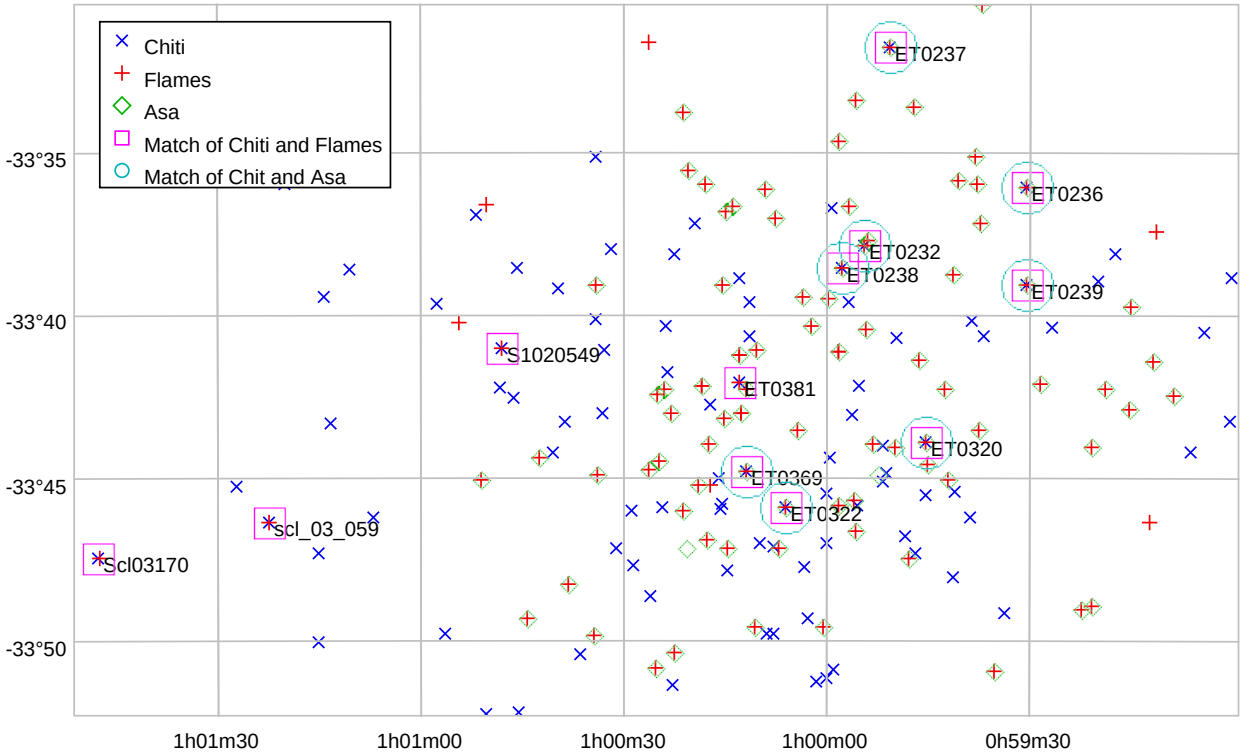

Figure 2: Sky coordinates match of Chiti, FLAMES, and Asa using a matching radius of 2 arcseconds.

Using the matching process described, we found 12 matched stars between Chiti and FLAMES data sets. Between Chiti and Asa we found 8 matched stars, that are the same as matched stars between Chiti and FLAMES. There is a high degree of agreement between FLAMES and Asa stars. The data set of Asa has a smaller field of view, that could partly explain the 4 stars that were matched between Chiti and FLAMES, but not matched between Chiti and Asa. In order to ensure the accuracy of the matching process, we repeated the same process for different matching radii from 1 arcsecond to 18 arcseconds, or 0.005 degrees. We only find additional matches at 18 arcseconds, where we find 15 matched stars between the FLAMES and Chiti data sets. Considering the accuracy of the skycoordinates, it is likely these additional matched stars are coincidental. We are therefore confident we have not missed any matched stars within the matched data sets.

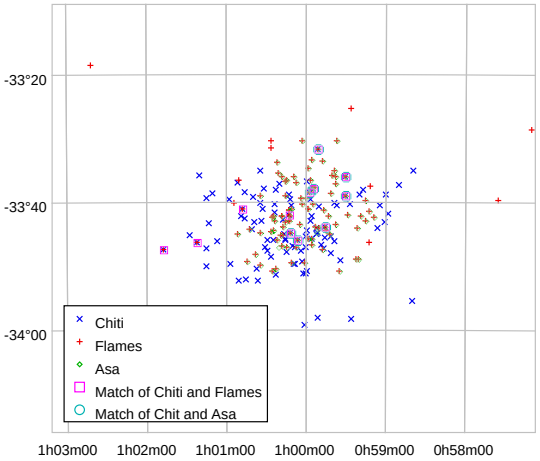

(a) Full field of view of the different data sets on Sculptor Dwarf Galaxy

(b) The Sculptor Dwarf Galaxy, from the 2.2-metre MPG/ESO telescope at ESO's La Silla Observatory. Credit:ESO

Figure 3: Sculptor dwarf Galaxy in the sky

As the data sets use different naming conventions for their stars, we will try to use FLAMES and Asa's numbered convention as consistently as possible. Important to note is that these data sets do not fully overlap, as Chiti et al. (2018) includes much fainter stars. We can also use Chiti's date-style names in cases where this is suitable.

FLAMES(Hill)	Asa	Chiti
ET0232	232	7_4_1514
ET0236	236	7_4_2408
ET0237	237	7_3_243
ET0238	238	11_1_2583
ET0239	239	11_1_4824
ET0320	320	11_1_3738
ET0322	322	10_8_3315
ET0369	369	10_8_2908
Scl03170		10_8_61
ET0381		10_8_2818
Scl_03_059		10_8_320
S1020549		10_8_1072

Table 1: Matched stars names

3.2 Carbon estimates

The data set from Asa contained two different [C/Fe] estimates. The differences in these values follow from different assumptions in calculating the Carbon abundance.

For all the figures in this paper, we use the [C/Fe] estimate using the assumption of [N/Fe] = 0 in order to match the results in Skúladóttir et al. (2015). The difference between these two methods is shown in figure 4.

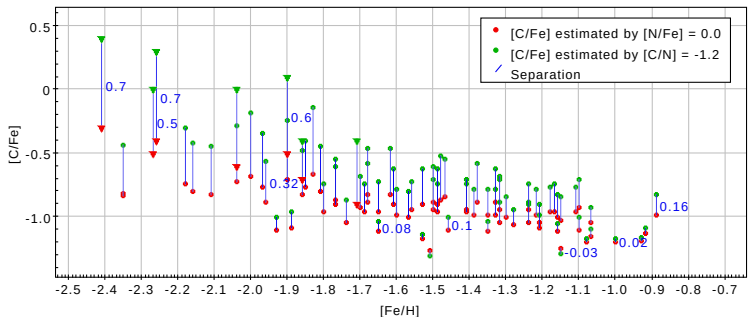

Figure 4: Difference in [C/Fe] estimates versus [Fe/H]
The [C/Fe] estimate assuming [C/N] = -1.2 (green circles), is higher over all [Fe/H] than the [C/Fe] estimate assuming [N/Fe] = 0.0 (red circles).

The difference in [C/Fe] is relatively small, but the two estimates diverge at lower metallicities.

3.3 Luminosity calculations

According to Salvadori et al. (2015), the classical way to determine if a stellar population contains CEMP stars is to plot the [C/Fe] versus Log(L/L$\odot$) of the population, and compare the results to the definition of CEMP stars by Aoki et al. (2007), which we have mentioned in section 2.2. Chiti et al. (2018) did not make this traditional Aoki diagram, and their data also does not include luminosities, but only photometry of the V-band, and B-band. In order to make an Aoki plot for the Chiti data, we calculated the luminosties from the magnitude in the V-band using equation 4 to calculate absolute magnitudes, and then using equation 5 to find the Log of luminosity over solar luminosity.

$$M = m - 5 * Log(d/10pc) - BC \tag{4}$$

$$Log(L/L\odot) = 0.4 * (M\odot - M) \tag{5}$$

$d = 86kpc \pm 5kpc$ (de Boer et al., 2011)
$M\odot = 4.83$ NASA
$BC = -0.495$ (Bolometric correction) (Alonso et al., 1999)

Despite our best efforts, results of the Log(L/L⊙) for Chiti and Asa, that did have luminosities in the data sets differ slightly. This is likely due to a different band being used for the luminosity calculation. In order to clarify our results, we match both Chiti data sets and Asa data sets with a data set from Gaia eDR3 (Brown et al., 2021). This results in 47 matches with the Chiti data set, and 7 matches with the Asa data set. We can then use the G-band magnitude provided within the Gaia data set to arrive at a consistent luminosity to plot both the Chiti and Asa data sets with.

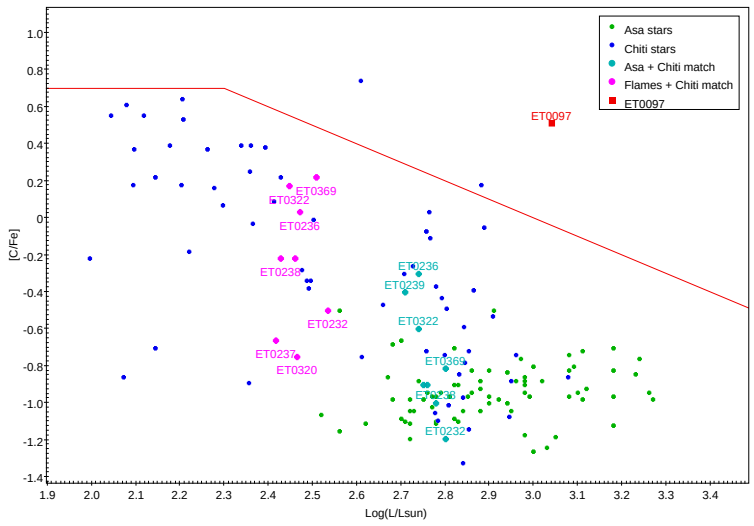

Figure 5: [C/Fe] versus Log(L/L⊙)
Aoki diagram of Chiti (blue) and Asa (green) stars. The matched stars show the difference in [C/Fe] measured by Chiti and Asa, but also show that our luminosities are different. Our resulting plot from matching the Chiti and Asa data sets with Gaia data in order to use consistent luminosities is show in section 4.2.

4 Results

4.1 Comparison of Carbon measurements

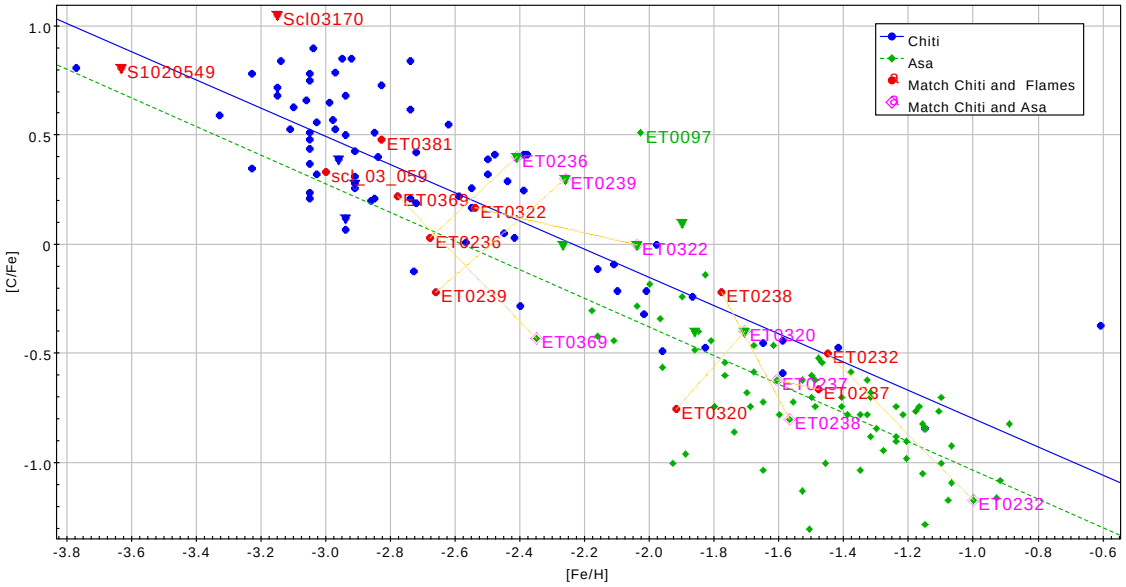

Figure 6: [C/Fe] versus [Fe/H]
Chiti data set (blue circles) use their measured [C/Fe], and Asa data set (green diamonds) uses [C/Fe] estimates assuming [N/Fe] = 0. Some stars do not have [C/Fe] estimates, but only have known upper boundaries for their [C/Fe] (Triangles). The 12 matched stars between Chiti and FLAMES (red circles) use the [C/Fe] and [Fe/H] values from Chiti. The 8 matched stars between Chiti and Asa (purple diamonds) use [C/Fe] and [Fe/H] values from Asa. The 8 same stars that are doubly matched, are connected with yellow relation lines. The solid blue line is the linear fit to the Chiti data, whereas the dotted green line is the linear fit to the Asa data.

Describing figure 6

An inverse trend was found between [C/Fe] and [Fe/H], showing that the lower metallicity stars have relatively high Carbon over Iron abundances. The Chiti data set generally found more low [Fe/H] stars, as well as finding lower minimal [Fe/H] at ~ -3.2 with two outliers at [Fe/H] ~ -3.7 compared to Asa's minimal [Fe/H] of ~ -2.4.

When we compare the 8 doubly matched stars, we notice that most of the matched stars have both a lower [Fe/H] and higher [C/Fe] when using the Chiti data, confirming a consistent difference in measurements where Chiti data is shifted along the trend. The mean shift of Asa [Fe/H] - Chiti [Fe/H] = 0.2925. The exceptions to this

Matched star	ET0232	ET0236	ET0237	ET0238	ET0239	ET0320	ET0322	ET0369
[Fe/H] Asa - Chiti	0.45	0.27	-0.13	0.21	0.4	0.21	0.5	0.43

shift along the trend; ET0236, ET0239, and ET0320, are all still shifted towards lower iron abundances, but also show lower [C/Fe] measurements instead of higher. For these 3 stars the Asa [C/Fe] values used were upper bounds of their [C/Fe], and not [C/Fe] estimates. It is possible this explains the lower measurements in the Chiti data.

The 4 matched stars that were only matched to FLAMES stars also turn out to to be the most metal-poor, and have the highest [C/Fe] values. Though S1020549 and Scl03170 [C/Fe] were only known as upper boundaries. Meaning, their [C/Fe] might well be lower should measurements be made.

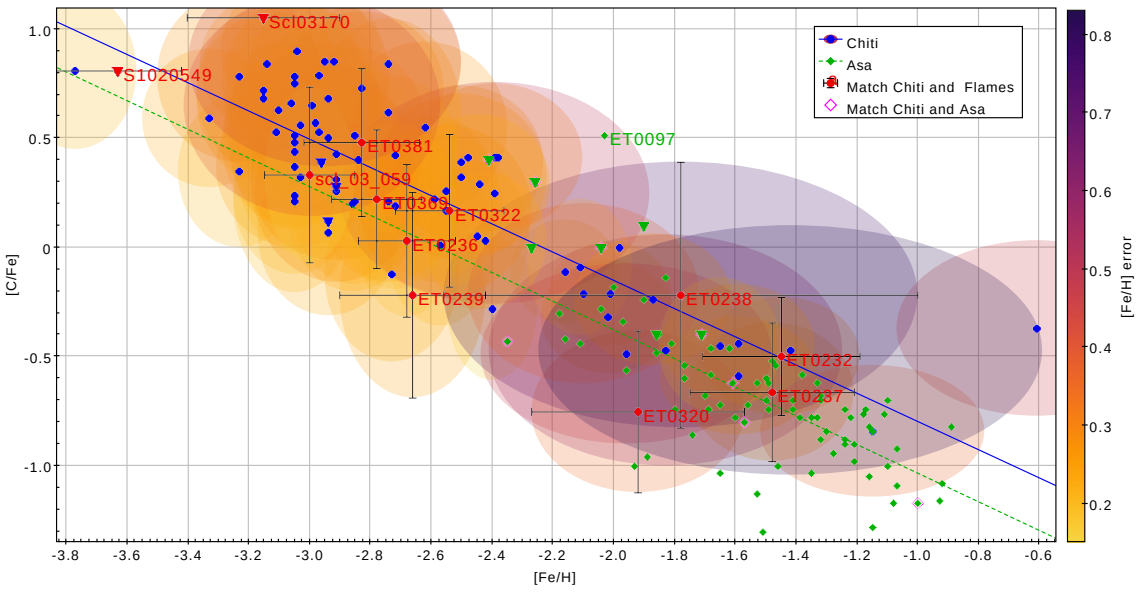

Figure 7: [C/Fe] versus [Fe/H] including error values
The black error-bars are shown for the 12 matched stars between Chiti and FLAMES, using. The colors of the spectrum in the sidebar show the magnitude of the error in [Fe/H] plotted as elliptical areas with a size of errors in [C/Fe] and [Fe/H]. For Carbon upper bounds; the triangles as explained in figure 6, no [C/Fe] error values are available.

There seems to be a systematic offset between Chiti [C/Fe] and [Fe/H] compared to FLAMES and Asa. However, as we can see in figure 7, the errors in these measurements are large.

4.2 Aoki diagrams

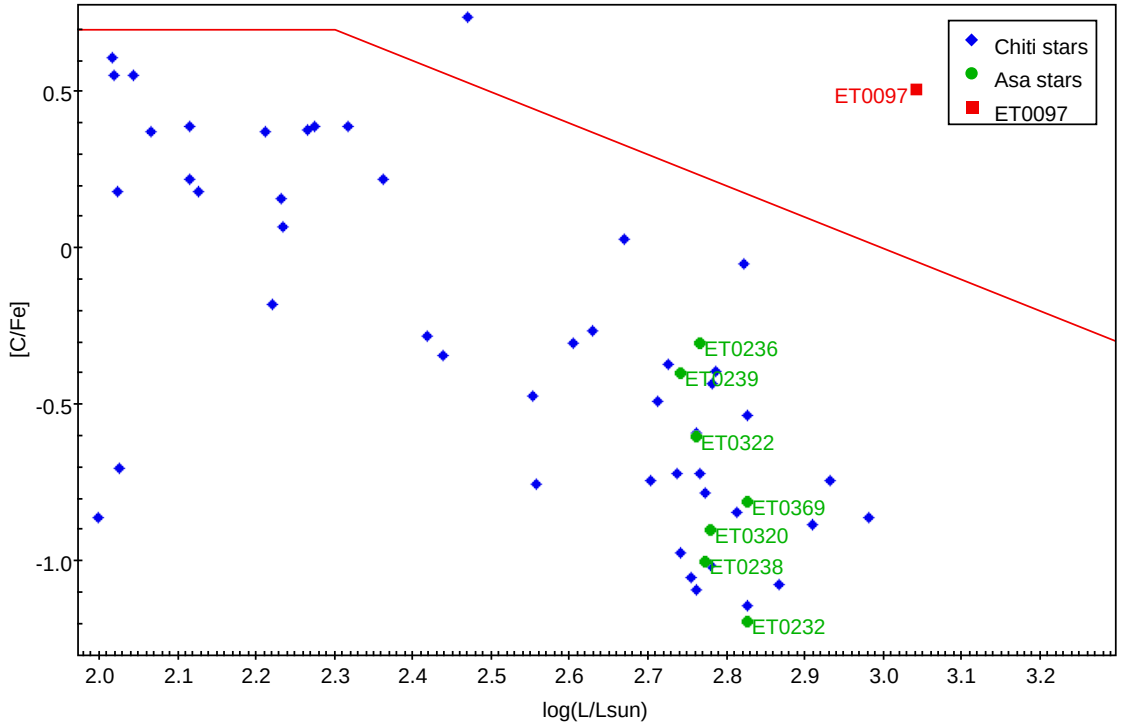

Figure 8: [C/Fe] versus Log(L/L⊙).
Aoki diagram of Chiti and Asa stars using luminosities from the Gaia data set (Brown et al., 2021). The red line indicates the definition of CEMP stars from Aoki et al. (2007).
1. [C/Fe] $\geq +0.7$ for stars with $\log(L/L_\odot) \leq 2.3$
2. [C/Fe] $\geq +3.0 - \log(L/L_\odot)$ for stars with $\log(L/L_\odot) > 2.3$
Chiti stars (blue diamonds) and Asa stars (green circles) fall largely under the CEMP barrier. With the exception of 1 Chiti star, and ET0097 (red square) which was previously found by Skúladóttir et al. (2015), and is included as a reference.

In figure 9b we replot the Chiti data set stars in relation to stars from the Galactic Halo (Frebel and Norris, 2013).

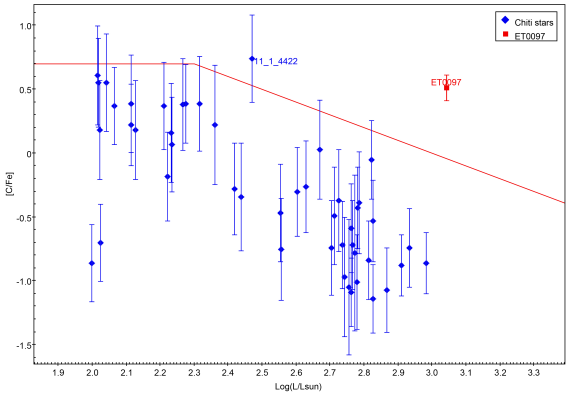

(a) Aoki diagram of Chiti stars with [C/Fe] error margins. Asa's star; ET0097 (red square) for reference.

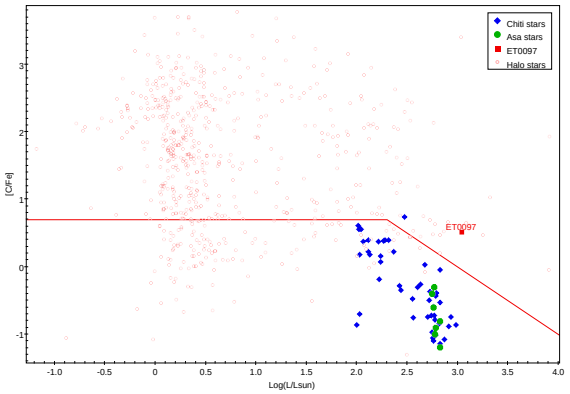

(b) Aoki diagram of Chiti stars (blue circles), Asa stars (green diamonds) and Halo stars (pink open circles) from Frebel et al.

Figure 9: Aoki diagrams of Sculptor stars

4.3 Abundances of marker chemicals

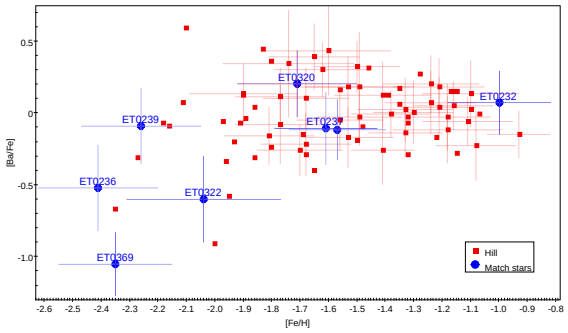

Figure 10: [Ba/Fe] vs [Fe/H] FLAMES (red circles) and Chiti matched stars (blue circles).

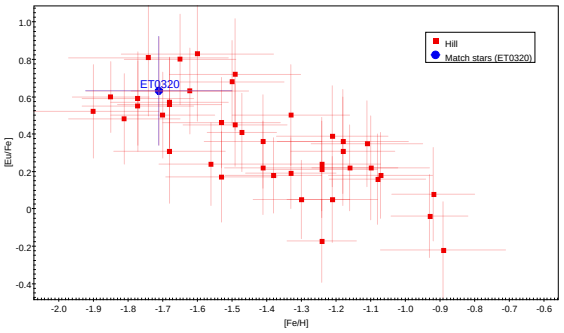

Figure 11: [Eu/Fe] vs [Fe/H] FLAMES (red circles) and Chiti matched stars (blue circles).

The FLAMES data set contains chemical abundances for elements that were not measured by Chiti et al. (2018). There are 8 stars that we have matched between the Chiti and FLAMES data that FLAMES has [Ba/Fe] values for, and 1 of those matched stars also has a [Eu/Fe] value. Barium and Europium are markers used to determine if a CEMP star classifies as a CEMP-r, CEMP-s, or CEMP-no star, as we have discussed in section 2.2. The values we find for the Chiti matched stars are compatible with CEMP-no star values. [Ba/Fe] on all matched stars is well under

a value of 1, and [Eu/Fe] on the only matched star we have a measurement of 0.63 < 1. However, in figure 9b, we see that none of these stars are above the defining red line in our Aoki diagram, and do not classify as CEMP stars in the first place under this definition.

5 Discussion

Our aim is to compare the results from Chiti et al. (2018) with Skúladóttir et al. (2015) and FLAMES (Hill et al., 2019) and specifically evaluate the CEMP fraction in the Sculptor dSph Galaxy. We compare measurements for same stars and also determine whether stars classify as CEMP stars.

Our comparison plots of [Fe/H] vs. [C/Fe] show Chiti et al. (2018) has higher abundances, in both Iron and Carbon, than the literature on Sculptor, across all matched stars. The exception are stars that had [C/Fe] known only to an upper bound. We are careful to draw any conclusions, as the errors in both [Fe/H] and [C/Fe] are significant. More accurate measurements, or a greater number of matched stars, is required to show if there is a statistical offset.

Additionally, when we plot Chiti's sample in an Aoki diagram to check if any of their stars were measured to be CEMP stars, we find only 1 new CEMP star. In figure 9a we have plotted the results for both Chiti's data, Asa's data, and a data set by Frebel and Norris (2013) on the EMP stars of the Milky way Halo in an Aoki diagram. Chiti's paper did not include an Aoki diagram, but stated a CEMP fraction of 36% for stars of [Fe/H] $= -3.0$ or less.

This means that according to the definition by Aoki et al. (2007) for CEMP stars, the CEMP fraction out of Chiti's sample is much lower than stated in the Chiti et al. (2018) paper, at 1 CEMP star out of 100 total. Figure 9b makes it clear that the [C/Fe] in EMP stars of the Halo of our Milky way is markedly different compared to the EMP population of the Sculptor dwarf Galaxy. Chiti's likening of their Sculptor CEMP fraction to that of the Milky Way Halo is not supported by our results. We find that the Aoki diagram for Sculptor stars looks very different from the Aoki diagram for Halo stars.

This might point to different origins or processes within these respective formation locations at early times. It is an indicator that EMP stars have various properties that we can further study. The low CEMP fraction we find in Sculptor is in alignment with the belief that CEMP-no stars are relatively rare in our Galactic neighborhood.

We cannot explain the cause of the discrepancy between Chiti's results and our matched star plots. We didn't directly compare their methods, but only their results. Chiti et al. (2018) used a different definition for their CEMP stars that ignores luminosity. We chose to use the definition in Aoki et al. (2007), as it incorporates the effects of evolution along the giant branch on carbon abundances (Aoki et al., 2007).

We are further limited by the relatively small sample of matched stars at 12 between Chiti et al. (2018) and FLAMES (Hill et al., 2019), and 8 between Chiti et al. (2018)

and Skúladóttir et al. (2015). which is a very low sample size.

We can not accurately assess whether the Chiti et al. (2018) CEMP star candidate; 11_1_4422, is a true CEMP-no star due to the large error margins in their [C/Fe] values, as is shown in figure 9a. This star is not included in our matched stars between Chiti et al. (2018) and FLAMES (Hill et al., 2019), so we also do not know its [Ba/Fe] and [Eu/Fe].

The methodology we used for the matching process has likely found all possible same stars within the Chiti, FLAMES and Asa data sets. We have checked the matching process with the high degree of agreement between the sky coordinates of Asa and FLAMES, and again with the iterative matching radius mentioned in section 3.1. However, Chiti et al. (2018) measured stars up to lower metallicities than both FLAMES and Asa. It is possible that future observations on Sculptor dSph Galaxy can take more spectroscopic measurements on chemical abundances for the stars Chiti et al. (2018) have found.

The [C/Fe] values we have used for Skúladóttir et al. (2015) were estimates using the assumption of [N/Fe] = 0. The alternative were estimates using the assumption of [C/N] = -1.2, and would have resulted in marginally higher [C/Fe] values, that are higher still towards lower metallicty values. In combination with the large margins of error on the [C/Fe] estimates, our comparison of [C/Fe] from Chiti et al. (2018) and Skúladóttir et al. (2015) becomes less certain.

The luminosities we calculate for the Chiti data set do not correspond precisely with the luminosities in the Asa data set. We did apply a Bolometric correction from Alonso et al. (1999), but may have still used a different spectroscopic band. We used G-band data from a match of our Sculptor stars and the Gaia mission Brown et al. (2021) to get corresponding luminosities for both Chiti and Asa. In doing so, we reduced the size of our data set to only 47 stars matched between Chiti and Gaia data, and 7 matched stars between Asa and the Gaia data set. As this only shifted the luminosities slightly, there are no differences in the number of CEMP stars.

A statistical analysis on the [C/Fe] and [Fe/H] could help to quantify these uncertainties so that we can indicate the existence of a signifcant statistical shift in the [C/Fe] data between Chiti and Asa. However, this is left for future work, due to the small sample size of matched stars.

More matches between different research groups of Sculptor stars need to be found combining their data on known stars, and averaging out differences in methodology (Mainly on determining [C/Fe]).

A standardized naming convention used by different research groups would be of great aid in comparing measurements between research groups.

6 Conclusion

This research compared the recent findings of Chiti (Chiti et al., 2018) on MP, EMP and CEMP stars within Sculptor dSph to that of previous research, mainly Asa (Skúladóttir et al., 2015) and FLAMES (Hill et al., 2019).

The apparent discrepancy between Chiti and both Asa and FLAMES was investigated by identifying matched stars within the respective data sets, and plotting the [C/Fe] of these match stars in relation to [Fe/H]. We then compared the CEMP fraction of the Sculptor dwarf Galaxy by plotting an Aoki diagram for the Chiti sample.

We found 12 match stars when matching Chiti and FLAMES, and 8 doubly matched stars between Chiti and Asa. These match stars were shifted towards lower [Fe/H] and higher [C/Fe] in Chiti's sample compared to FLAMES and Asa. Using an Aoki diagram, we found 1 CEMP candidate within Chiti's sample.

The single CEMP candidate indicates an unlikely CEMP fraction similar to that of the Galactic Halo. Our results oppose the findings of a 36% CEMP fraction for stars with [Fe/H] $<$ -3.0 in the Sculptor dsph Galaxy.

Galactic paleontology allows us to be able to place constraints on the processes and environment of the early universe. Sculptor dSph Galaxy provides interesting opportunities to study EMP stars outside of the Galactic Halo environment. Additional efforts in observations and research on Sculptor should be made in order to further our understanding.

7 Bibliography

References

Alonso, A., Arribas, S., and Martínez-Roger, C. (1999). ADS. *Astronomy and Astrophysics Supplement, v.140, p.261-277*, 140:261.

Aoki, W., Beers, T. C., Christlieb, N., Norris, J. E., Ryan, S. G., and Tsangarides, S. (2007). Carbon-enhanced Metal-poor Stars. I. Chemical Compositions of 26 Stars∗. *Astrophys. J.*, 655(1):492–521.

Brown, A. G. A., Vallenari, A., Prusti, T., de Bruijne, J. H. J., Babusiaux, C., Biermann, M., Creevey, O. L., Evans, D. W., Eyer, L., Hutton, A., Jansen, F., Jordi, C., Klioner, S. A., Lammers, U., Lindegren, L., Luri, X., Mignard, F., Panem, C., Pourbaix, D., Randich, S., Sartoretti, P., Soubiran, C., Walton, N. A., Arenou, F., Bailer-Jones, C. A. L., Bastian, U., Cropper, M., Drimmel, R., Katz, D., Lattanzi, M. G., van Leeuwen, F., Bakker, J., Cacciari, C., Castañeda, J., De Angeli, F., Ducourant, C., Fabricius, C., Fouesneau, M., Frémat, Y., Guerra, R., Guerrier, A., Guiraud, J., Piccolo, A. J.-A., Masana, E., Messineo, R., Mowlavi, N., Nicolas, C., Nienartowicz, K., Pailler, F., Panuzzo, P., Riclet, F., Roux, W., Seabroke, G. M., Sordo, R., Tanga, P., Thévenin, F., Gracia-Abril, G., Portell, J., Teyssier, D., Altmann, M., Andrae, R., Bellas-Velidis, I., Benson, K., Berthier, J., Blomme, R., Brugaletta, E., Burgess, P. W., Busso, G., Carry, B., Cellino, A., Cheek, N., Clementini, G., Damerdji, Y., Davidson, M., Delchambre, L., Dell'Oro, A., Fernández-Hernández, J., Galluccio, L., García-Lario, P., Garcia-Reinaldos, M., González-Núñez, J., Gosset, E., Haigron, R., Halbwachs, J.-L., Hambly, N. C., Harrison, D. L., Hatzidimitriou, D., Heiter, U., Hernández, J., Hestroffer, D., Hodgkin, S. T., Holl, B., Janßen, K., de Fombelle, G. J., Jordan, S., Krone-Martins, A., Lanzafame, A. C., Löffler, W., Lorca, A., Manteiga, M., Marchal, O., Marrese, P. M., Moitinho, A., Mora, A., Muinonen, K., Osborne, P., Pancino, E., Pauwels, T., Petit, J.-M., Recio-Blanco, A., Richards, P. J., Riello, M., Rimoldini, L., Robin, A. C., Roegiers, T., Rybizki, J., Sarro, L. M., Siopis, C., Smith, M., Sozzetti, A., Ulla, A., Utrilla, E., van Leeuwen, M., van Reeven, W., Abbas, U., Aramburu, A. A., Accart, S., Aerts, C., Aguado, J. J., Ajaj, M., Altavilla, G., Álvarez, M. A., Cid-Fuentes, J. Á., Alves, J., Anderson, R. I., Varela, E. A., Antoja, T., Audard, M., Baines, D., Baker, S. G., Balaguer-Núñez, L., Balbinot, E., Balog, Z., Barache, C., Barbato, D., Barros, M., Barstow, M. A., Bartolomé, S., Bassilana, J.-L., Bauchet, N., Baudesson-Stella, A., Becciani, U., Bellazzini, M., Bernet, M., Bertone, S., Bianchi, L., Blanco-Cuaresma, S., Boch, T., Bombrun, A., Bossini, D., Bouquillon, S., Bragaglia, A., Bramante, L., Breedt, E., Bressan, A., Brouillet, N., Bucciarelli, B., Burlacu, A., Busonero, D., Butkevich, A. G.,

Buzzi, R., Caffau, E., Cancelliere, R., Cánovas, H., Cantat-Gaudin, T., Carballo, R., Carlucci, T., Carnerero, M. I., Carrasco, J. M., Casamiquela, L., Castellani, M., Castro-Ginard, A., Sampol, P. C., Chaoul, L., Charlot, P., Chemin, L., Chiavassa, A., Cioni, M.-R. L., Comoretto, G., Cooper, W. J., Cornez, T., Cowell, S., Crifo, F., Crosta, M., Crowley, C., Dafonte, C., Dapergolas, A., David, M., David, P., de Laverny, P., De Luise, F., De March, R., De Ridder, J., de Souza, R., de Teodoro, P., de Torres, A., del Peloso, E. F., del Pozo, E., Delbo, M., Delgado, A., Delgado, H. E., Delisle, J.-B., Di Matteo, P., Diakite, S., Diener, C., Distefano, E., Dolding, C., Eappachen, D., Edvardsson, B., Enke, H., Esquej, P., Fabre, C., Fabrizio, M., Faigler, S., Fedorets, G., Fernique, P., Fienga, A., Figueras, F., Fouron, C., Fragkoudi, F., Fraile, E., Franke, F., Gai, M., Garabato, D., Garcia-Gutierrez, A., García-Torres, M., Garofalo, A., Gavras, P., Gerlach, E., Geyer, R., Giacobbe, P., Gilmore, G., Girona, S., Giuffrida, G., Gomel, R., Gomez, A., Gonzalez-Santamaria, I., González-Vidal, J. J., Granvik, M., Gutiérrez-Sánchez, R., Guy, L. P., Hauser, M., Haywood, M., Helmi, A., Hidalgo, S. L., Hilger, T., Hładczuk, N., Hobbs, D., Holland, G., Huckle, H. E., Jasniewicz, G., Jonker, P. G., Campillo, J. J., Julbe, F., Karbevska, L., Kervella, P., Khanna, S., Kochoska, A., Kontizas, M., Kordopatis, G., Korn, A. J., Kostrzewa-Rutkowska, Z., Kruszyńska, K., Lambert, S., Lanza, A. F., Lasne, Y., Le Campion, J.-F., Le Fustec, Y., Lebreton, Y., Lebzelter, T., Leccia, S., Leclerc, N., Lecoeur-Taibi, I., Liao, S., Licata, E., Lindstrøm, E. P., Lister, T. A., Livanou, E., Lobel, A., Pardo, P. M., Managau, S., Mann, R. G., Marchant, J. M., Marconi, M., Santos, M. M. S. M., Marinoni, S., Marocco, F., Marshall, D. J., Polo, L. M., Martín-Fleitas, J. M., Masip, A., Massari, D., Mastrobuono-Battisti, A., Mazeh, T., McMillan, P. J., Messina, S., Michalik, D., Millar, N. R., Mints, A., Molina, D., Molinaro, R., Molnár, L., Montegriffo, P., Mor, R., Morbidelli, R., Morel, T., Morris, D., Mulone, A. F., Munoz, D., Muraveva, T., Murphy, C. P., Musella, I., Noval, L., Ordénovic, C., Orrù, G., Osinde, J., Pagani, C., Pagano, I., Palaversa, L., Palicio, P. A., Panahi, A., Pawlak, M., Esteller, X. P., Penttilä, A., Piersimoni, A. M., Pineau, F.-X., Plachy, E., Plum, G., Poggio, E., Poretti, E., Poujoulet, E., Prša, A., Pulone, L., Racero, E., Ragaini, S., Rainer, M., Raiteri, C. M., Rambaux, N., Ramos, P., Ramos-Lerate, M., Fiorentin, P. R., Regibo, S., Reylé, C., Ripepi, V., Riva, A., Rixon, G., Robichon, N., Robin, C., Roelens, M., Rohrbasser, L., Romero-Gómez, M., Rowell, N., Royer, F., Rybicki, K. A., Sadowski, G., Sellés, A. S., Sahlmann, J., Salgado, J., Salguero, E., Samaras, N., Gimenez, V. S., Sanna, N., Santoveña, R., Sarasso, M., Schultheis, M., Sciacca, E., Segol, M., Segovia, J. C., Ségransan, D., Semeux, D., Shahaf, S., Siddiqui, H. I., Siebert, A., Siltala, L., Slezak, E., Smart, R. L., Solano, E., Solitro, F., Souami, D., Souchay, J., Spagna, A., Spoto, F., Steele, I. A., Steidelmüller, H., Stephenson, C. A., Süveges, M., Szabados, L., Szegedi-Elek, E., Taris, F., Tauran, G., Taylor, M. B., Teixeira, R., Thuillot, W.,

Tonello, N., Torra, F., Torra, J., Turon, C., Unger, N., Vaillant, M., van Dillen, E., Vanel, O., Vecchiato, A., Viala, Y., Vicente, D., Voutsinas, S., Weiler, M., Wevers, T., Wyrzykowski, Ł., Yoldas, A., Yvard, P., Zhao, H., Zorec, J., Zucker, S., Zurbach, C., and Zwitter, T. (2021). Gaia Early Data Release 3 - Summary of the contents and survey properties. *Astron. Astrophys.*, 649:A1.

Chiti, A., Simon, J. D., Frebel, A., Thompson, I. B., Shectman, S. A., Mateo, M., Bailey, J. I., Crane, J. D., and Walker, M. (2018). Detection of a Population of Carbon-enhanced Metal-poor Stars in the Sculptor Dwarf Spheroidal Galaxy$_*$. *Astrophys. J.*, 856(2):142.

Côté, B., Fryer, C. L., Belczynski, K., Korobkin, O., Chruślińska, M., Vassh, N., Mumpower, M. R., Lippuner, J., Sprouse, T. M., Surman, R., and Wollaeger, R. (2018). The Origin of r-process Elements in the Milky Way. *Astrophys. J.*, 855(2):99.

de Boer, T. J. L., Tolstoy, E., Saha, A., Olsen, K., Irwin, M. J., Battaglia, G., Hill, V., Shetrone, M. D., Fiorentino, G., and Cole, A. (2011). Deep wide-field imaging down to the oldest main sequence turn-offs in the Sculptor dwarf spheroidal galaxy. *Astron. Astrophys.*, 528:A119.

Frebel, A., Kirby, E. N., and Simon, J. D. (2010). Linking dwarf galaxies to halo building blocks with the most metal-poor star in Sculptor. *Nature*, 464(7285):72–75.

Frebel, A. and Norris, J. E. (2013). Metal-poor stars and the chemical enrichment of the universe. *Planets, Stars and Stellar Systems*, page 55–114.

Harwit, M. (1998). *Astrophysical Concepts*. Springer-Verlag, New York, NY, USA.

Hill, V., Skúladóttir, Á., Tolstoy, E., Venn, K. A., Shetrone, M. D., Jablonka, P., Primas, F., Battaglia, G., de Boer, T. J. L., François, P., Helmi, A., Kaufer, A., Letarte, B., Starkenburg, E., and Spite, M. (2019). VLT/FLAMES high-resolution chemical abundances in Sculptor: a textbook dwarf spheroidal galaxy. *Astron. Astrophys.*, 626:A15.

Jablonka, P., North, P., Mashonkina, L., Hill, V., Revaz, Y., Shetrone, M., Starkenburg, E., Irwin, M., Tolstoy, E., Battaglia, G., Venn, K., Helmi, A., Primas, F., and François, P. (2015). The early days of the Sculptor dwarf spheroidal galaxy. *Astron. Astrophys.*, 583:A67.

Kirby, E., Guo, M., Zhang, A., Deng, M., Cohen, J., Guhathakurta, P., Shetrone, M., Lee, Y., and Rizzi, L. (2015). Carbon in red giants in globular clusters and dwarf spheroidal galaxies. *The Astrophysical Journal*, 801.

Lardo, C., Battaglia, G., Pancino, E., Romano, D., de Boer, T. J. L., Starkenburg, E., Tolstoy, E., Irwin, M. J., Jablonka, P., and Tosi, M. (2016). Carbon and nitrogen abundances of individual stars in the Sculptor dwarf spheroidal galaxy. *Astron. Astrophys.*, 585(January 2016):A70.

McWilliam, A. (1997). ABUNDANCE RATIOS AND GALACTIC CHEMICAL EVOLUTION. *Annu. Rev. Astron. Astrophys.*, 35(1):503–556.

Salvadori, S., Skúladóttir, A., and Tolstoy, E. (2015). Carbon-enhanced metal-poor stars in dwarf galaxies. *Monthly Notices of the Royal Astronomical Society*, 454(2):1320–1331.

Sharma, M., Theuns, T., Frenk, C. S., and Cooke, R. J. (2018). Origins of carbon-enhanced metal-poor stars. *Mon. Not. R. Astron. Soc.*, 473(1):984–995.

Skúladóttir, Á. and Salvadori, S. (2020). Evidence for 4 Gyr timescales of neutron star mergers from Galactic archaeology. *Astron. Astrophys.*, 634:L2.

Skúladóttir, Á., Tolstoy, E., Salvadori, S., Hill, V., Pettini, M., Shetrone, M. D., and Starkenburg, E. (2015). The first carbon-enhanced metal-poor star found in the Sculptor dwarf spheroidal. *Astron. Astrophys.*, 574:A129.

Starkenburg, E., Hill, V., Tolstoy, E., Francois, P., Irwin, M. J., Boschman, L., Venn, K. A., de Boer, T. J. L., Lemasle, B., Jablonka, P., Battaglia, G., Groot, P., and Kaper, L. (2012). The extremely low-metallicity tail of the Sculptor dwarf spheroidal galaxy. *arXiv*.

Starkenburg, E., Hill, V., Tolstoy, E., González Hernández, J. I., Irwin, M., Helmi, A., Battaglia, G., Jablonka, P., Tafelmeyer, M., Shetrone, M., Venn, K., and de Boer, T. (2010). The NIR Ca ii triplet at low metallicity. Searching for extremely low-metallicity stars in classical dwarf galaxies. *Astron. Astrophys.*, 513:A34.

Taylor, M. B. (2005). TOPCAT & STIL: Starlink Table/VOTable Processing Software. *Astronomical Data Analysis Software and Systems XIV*, 347:29.

Taylor, M. B. (2006). STILTS - A Package for Command-Line Processing of Tabular Data. *Astronomical Data Analysis Software and Systems XV*, 351:666.

Tolstoy, E. (2011). Galactic paleontology. *Science*, 333, Issue 6039, pp. 176-178.

8 Appendix

8.1 Tables

For inquiries on the Tables used in this paper, please contact me via this e-mail: J.N.Wildering@student.rug.nl